Contents

1 Supplemental Figures

Figure S1: **Single cells produce IL-2 at a constant rate continuously over a timescale of hours.** Related to Figure 2,4. (A) $CD4^+$ T cell blasts were coated with an IL-2 capture matrix, reactivated using PMA and ionomycin, and seeded on an array of microscopic wells in the presence of fluorescently labeled anti-IL-2. Time-lapse images were taken every 5 minutes for 4 hours. Time-lapse images of IL-2 fluorescence on single IL-2 producers. (Scale bar = 10μ m.) (B) IL-2 accumulation dynamics on the single IL-2 producing cells shown in (A) . (C) More examples of IL-2 accumulation dynamics on single IL-2 producing cells. Data representative of 3 independent experiments.

Figure S2: **Single-cell signaling levels correspond to position within cytokine gradients.** Related to Figure 3.(A) Schematic of clusterwell plates. (B) Image of the Clusterwell plate. Differences in cytokine exposure reflect positional information in the plug. (C,D) Consumer-inert cell mixtures were sedimented over a layer of pre-stained $CD4^+$IL-2Rα^+ consuming cells. IL-2 was added on top such that some of the clusters became fully saturated with cytokine. The bottom layer of cells is only exposed to cytokine when the entire top plug is saturated. (E) To ensure that bulk depletion of IL-2 is not taking place, cells are prepared as in Fig.3, and left in a well mixed culture. (F) Calibration of flow cytometry measurements of cell fractions and microscopy measurement of cell density per $10^3\mu$m^3. The maximal density is 1.06 cells per $10^3\mu m^3$.

Figure S3: **A diffusion-consumption mechanism explains the formation of gradients in multiple cytokines.** Related to Figure 3. Diffusion-consumption mechanism describes cytokine penetration for multiple cytokines. (A) Experimental scheme: Cytokine consuming cells (Primary IL-2Rα^+ T cells for IL-2, CH12 for IL-4, and B16 melanoma for IFNγ) were loaded in the clusterwell plate and different concentrations (10nM, 1nM, and 100pM) of the relevant cytokine were added on top. As a control for bulk cytokine depletion, consuming cells were mixed with cytokine and left in suspension in a flat-bottom 96 well plate. After the system reaches steady-state ($\sim$1hr), cells were fixed and permeabilized for intracellular flow cytometric analysis of the relevant phosphorylated transcription factor (TF), pSTAT5, pSTAT6, and pSTAT1 respectively. (B) The response of IL-2Rα^+ $CD4^+$ T cells, CH12 cells, and B16 cells to different doses of IL-2, IL-4, and IFNγ respectively. The mean fluorescent intensity (MFI) follows a Hill function curve with Hill coefficient 1. (C) Distributions of the different pSTATs in consumers for different concentrations of cytokine. As the concentration of cytokine increases, it penetrates deeper into the cluster resulting in a larger fraction of TF^+ cells. Bulk cytokine depletion does not play a role, as evident by the dashed lines. (D) The $\%TF^+$ scales with the source concentration. As is predicted by the framework of diffusion and consumption, the scaling follows the relation $\%TF^+ \propto I\left(\frac{c_0}{EC_{50}}\right) = \int_{0.25}^{\frac{c_0}{EC_{50}}} \frac{d(C)}{2\sqrt{((C)-\ln(1+(C)))}}$ with 25% of the EC_{50} set as the threshold for signal detection. Where errors do not appear they are smaller than marker.

Figure S4: **Discrete niches of high cytokine concentration are formed around IL-2 producers** Related to Figure 4. (A) Additional examples of signaling micro domains around IL-2 producing cells imaged using a PlaneView device. (B) Staining controls: 10 layers of IL-2Rα^+ consuming cells, or a combination of 10% IL-2Rα^+ cells and 90% IL-2Rα^- filler cells are loaded on a PlaneView device. The cells are incubated with either media as a negative control or 10nM of IL-2 as a positive control. The cells are labeled for IL-2Rα and pSTAT5 for microscopy analysis.

Figure S5: **Boosting the T_{reg} compartment and experimental controls for figure 5.** Related to Figures 5,6 (A) Lymphoid organs from boosted mice were processed for intracellular staining of FoxP3. Cells were first gated as $CD4^+$, then FoxP3 was plotted versus IL-2Rα. Nearly all IL-2Rα+ cells are also FoxP3+. (B) Boosted B10.A mice were sequentially injected over 3 days with IL-2-α^-IL-2 complexes. Boosted mice exhibited a uniformly increased T_{reg} compartment size. (C) *left*: Negative and positive controls for pSTAT5 staining. A fraction of splenocytes was treated ex vivo with either IL-2 or JAKI inhibitor and pSTAT5 was measured by flow cytometry. *center and right:* pSTAT5 distributions were analyzed for IL-2 i.c. boosted and wild type mice. To control for non-specific IL-2 production, B10.A mice were adoptively transferred with $3 \cdot 10^6$ 5C.C7 *Il-2*$^{-/-}$ $CD4^+$ cells and immunized. Lymph nodes and spleens were processed and analyzed for pSTAT5 by flow cytometry. Bar plots are data from an experiment with three mice per group.

Figure S6: **Verification of equal IL-2 production in boosted and wild type mice.** Related to Figures 5,6. 6 hours P.I. mice were euthanized and a fraction of the lymph nodes and spleens was immediately taken for IL-2 secretion assays. IL-2 production among adoptively transferred cells was measured. (A) Wild type and Boosted mice received roughly equivalent numbers of $CD4^+$ 5C.C7 cells. (B) Activation of the cells, measured by the fraction of IL-2 producers, was unaffected by the boosting of the T_{reg} compartment. *Bottom* Positive and negative controls for IL-2 secretion assay: IL-2 detection was then preformed on cultured cells with fresh media (Negative control) or with media containing IL-2 (Positive control).

Oyler-Yaniv et al. Figure S1

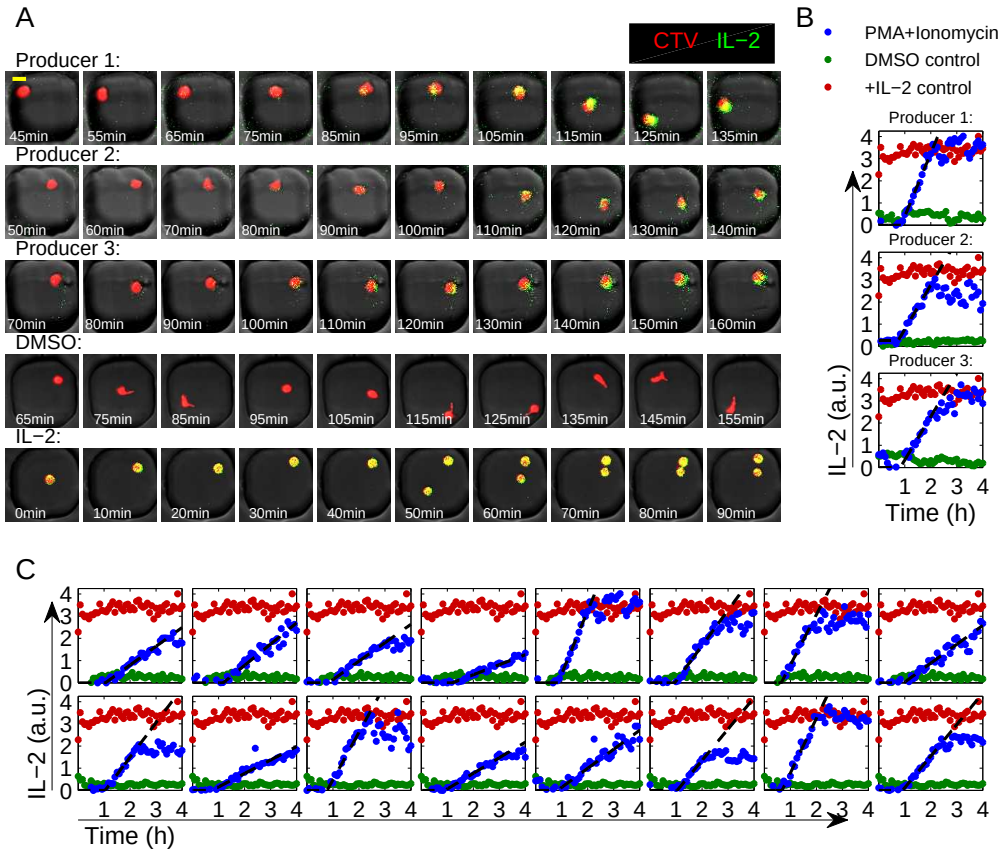

Oyler-Yaniv et al. Figure S2

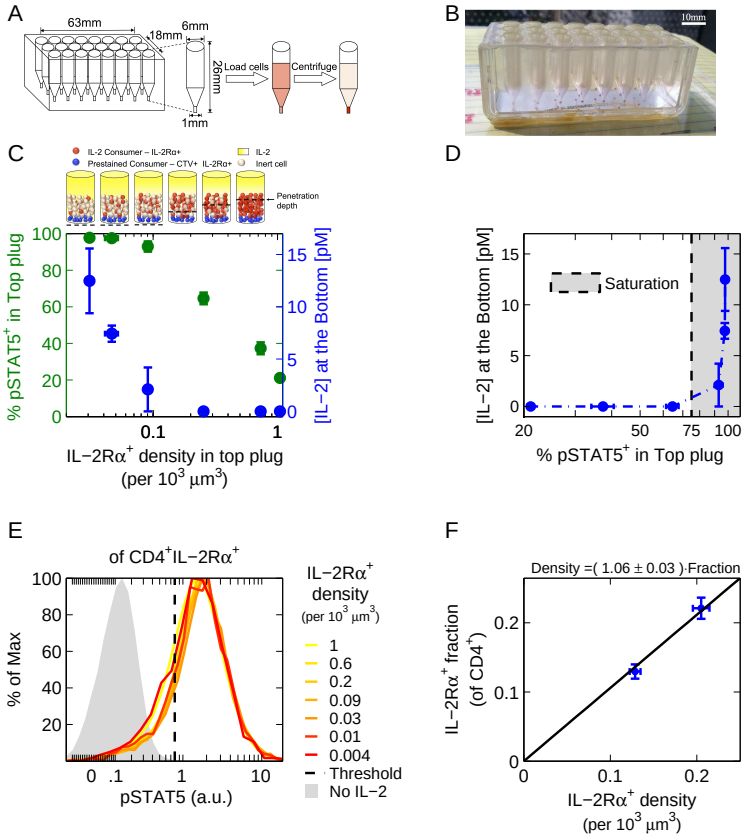

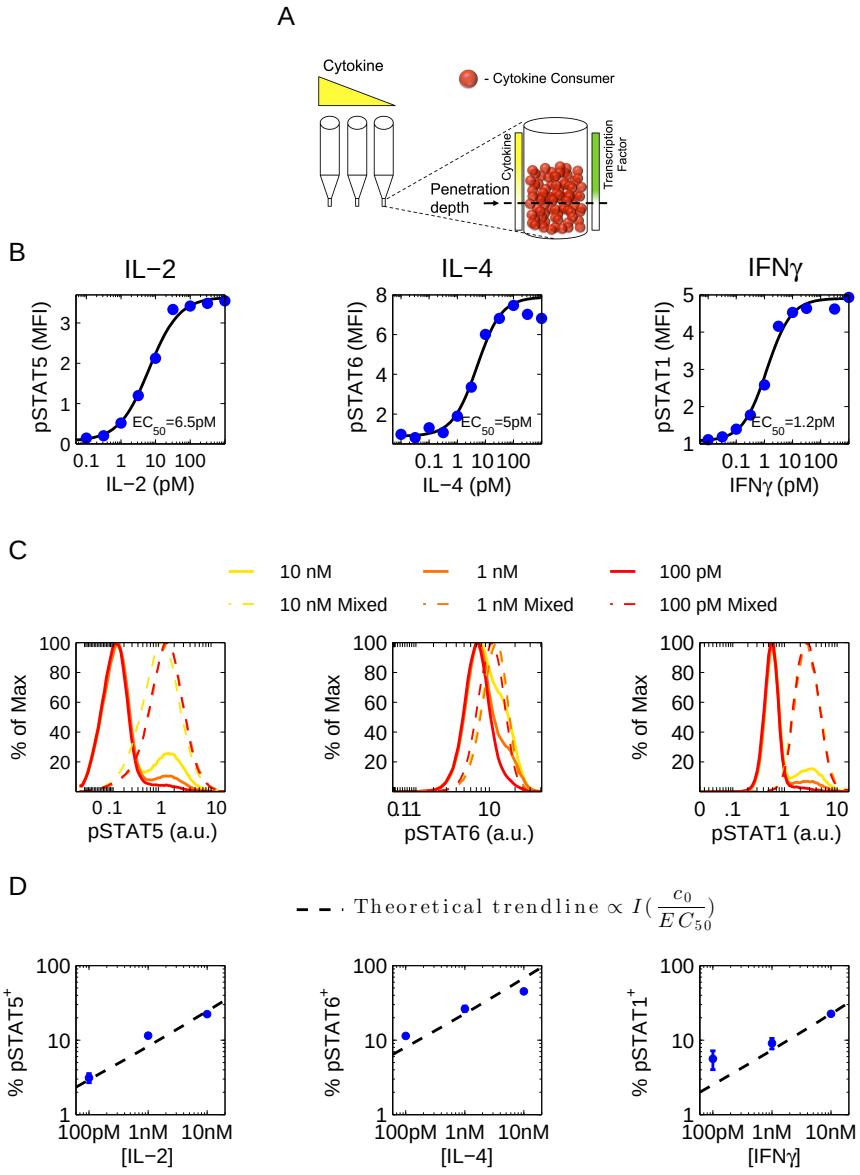
A
Cytokine
- Cytokine Consumer
Cytokine
Transcription Factor
Penetration depth
B
IL−2
IL−4
IFNγ
pSTAT5 (MFI)
pSTAT6 (MFI)
pSTAT1 (MFI)
EC50=6.5pM
EC50=5pM
EC50=1.2pM
IL−2 (pM)
IL−4 (pM)
IFNγ (pM)
C
10 nM
10 nM Mixed
1 nM
1 nM Mixed
100 pM
100 pM Mixed
% of Max
pSTAT5 (a.u.)
pSTAT6 (a.u.)
pSTAT1 (a.u.)
D
Theoretical trendline ∝ I(c0/EC50)
% pSTAT5+
% pSTAT6+
% pSTAT1+
100pM 1nM 10nM
[IL−2]
[IL−4]
[IFNγ]

Oyler-Yaniv et al. Figure S4

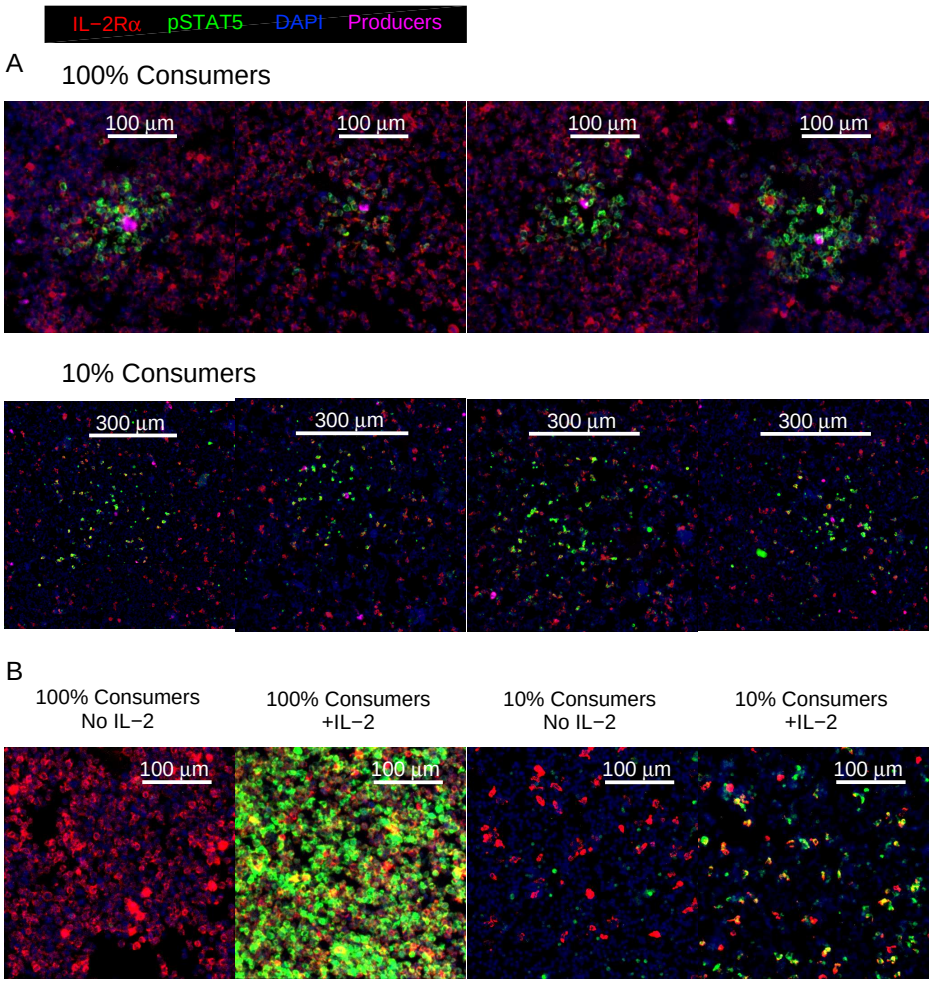

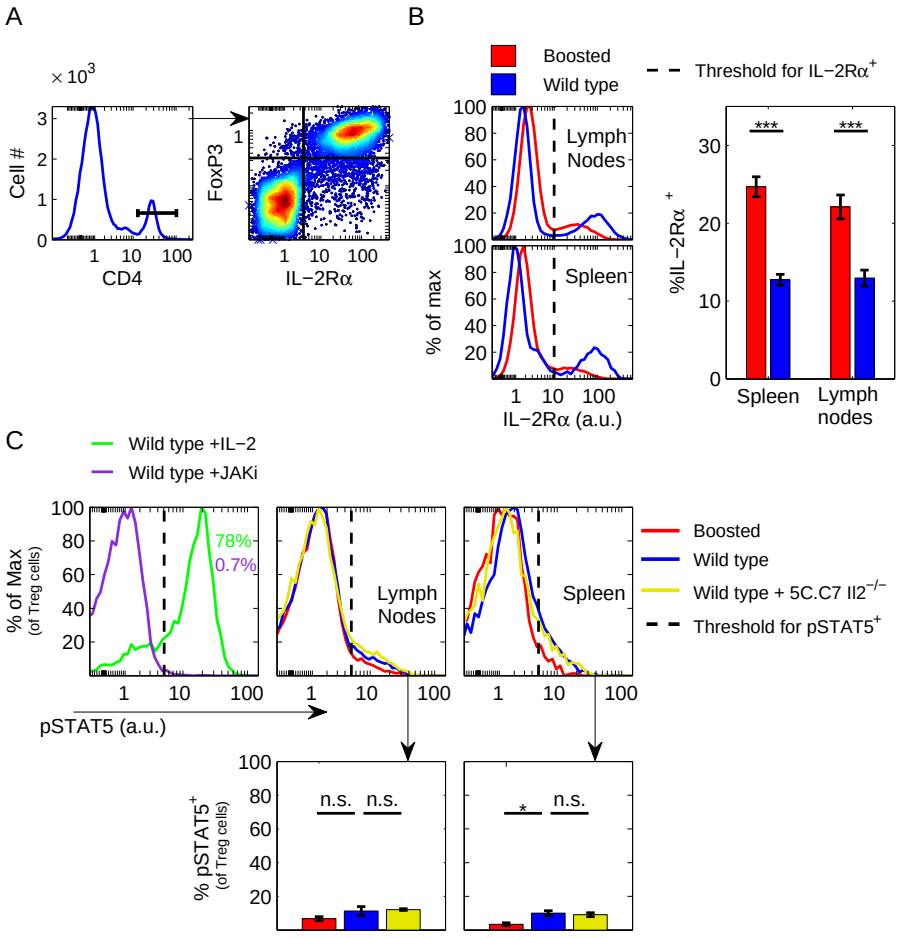
A
B
C
Cell #
CD4
FoxP3
IL−2Rα
Boosted
Wild type
Threshold for IL−2Rα+
Lymph Nodes
Spleen
% of max
IL−2Rα (a.u.)
%IL−2Rα+
Spleen
Lymph nodes
Wild type +IL−2
Wild type +JAKi
78%
0.7%
% of Max
(of Treg cells)
pSTAT5 (a.u.)
Wild type + 5C.C7 Il2−/−
Threshold for pSTAT5+
% pSTAT5+
(of Treg cells)
n.s.
*

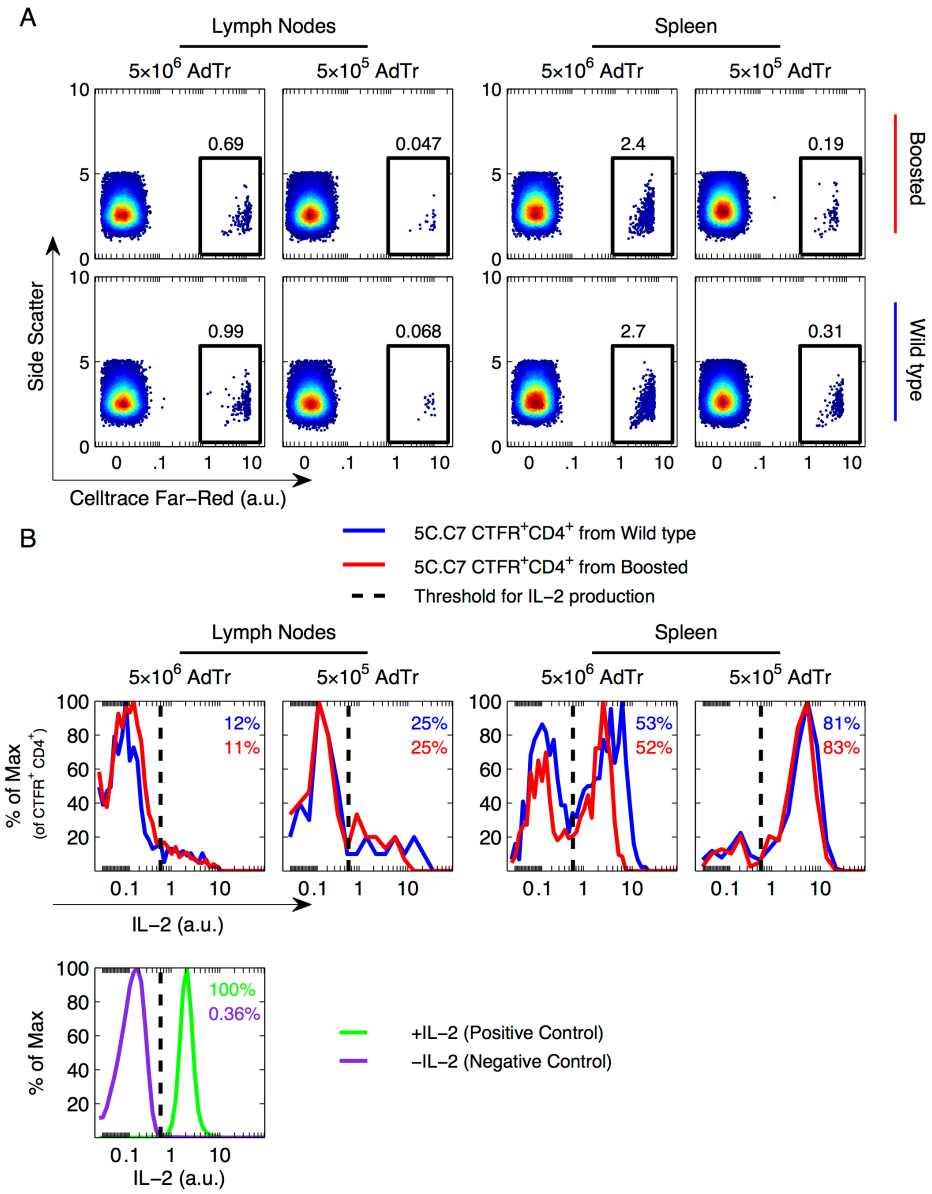
A
Lymph Nodes
Spleen
5×10^6 AdTr
5×10^5 AdTr
0.69
0.047
2.4
0.19
0.99
0.068
2.7
0.31
Boosted
Wild type
Side Scatter
Celltrace Far–Red (a.u.)
B
5C.C7 CTFR+CD4+ from Wild type
5C.C7 CTFR+CD4+ from Boosted
Threshold for IL–2 production
% of Max
(of CTFR+ CD4+)
12%
11%
25%
25%
53%
52%
81%
83%
IL–2 (a.u.)
100%
0.36%
+IL–2 (Positive Control)
–IL–2 (Negative Control)

2 Mathematical Framework: Diffusion-Consumption systems

2.1 Paracrine signaling - General description

We begin with a general model of cytokine diffusion and consumption. A cytokine is released from a source and freely diffuses away. Eventually, the cytokine molecule binds to a cell carrying the appropriate receptor and gets endocytosed. Initially, the model assumptions are only that cells do not directly affect each other's consumption ability (**linearity in n, the concentration of cells**). At this point we do not assume any particular concentration dependence for the per-cell consumption rate and write it as $k_{\text{consumption}} f(c)$ where $k_{\text{consumption}}$ is a kinetic consumption rate (for the whole cell) and $f(c)$ is a (monotonous) function of concentration. The diffusion-consumption equation is:

$$\frac{\partial c}{\partial t} = \mathcal{D}\nabla^2 c - n_{\text{consumers}} k_{\text{consumption}} f(c). \tag{1}$$

Next, we take the steady-state limit $\frac{\partial c}{\partial t} \to 0$ of this equation:

$$0 = \nabla^2 c - \frac{n_{\text{consumers}} \cdot k_{\text{consumption}}}{\mathcal{D}} \cdot f(c). \tag{2}$$

We define the screening length $\lambda^2_{\text{niche}} = \frac{\mathcal{D}}{k_{\text{consumption}} \cdot n_{\text{consumers}}}$ and rescale $\tilde{r} = \frac{r}{\lambda_{\text{niche}}}$. $\tilde{\nabla}$ is the del operator in the dimensionless rescaled distance units.

$$0 = \tilde{\nabla}^2 c - f(c). \tag{3}$$

Using the quasi-stationary limit is justified by considering the timescales of these processes: Cytokine production and cytokine receptor expression levels change over the timescale of hours (Fig. S3, Huang et al. (2013); Helmstetter et al. (2015); Tkach et al. (2014); Sojka et al. (2004); Janský et al. (2003); Boyman and Sprent (2012)). The cellular composition of tissue changes during an immune response over the timescales of days (Fig.1, Murphy (2011); Jacob (1991)). The *relaxation time*, the timescale over which the gradient is formed, is dominated by the mean first-passage time, the time the fastest moving molecules arrives at a specific location and is therefore linearly dependent on the distance from the sourceGregor et al. (2007); Kolomeisky (2011), a behavior we also observed in our simulations of approach to steady state, and calculations of relaxations time which is in the order of a few minutes. Taking these together justifies our approach.

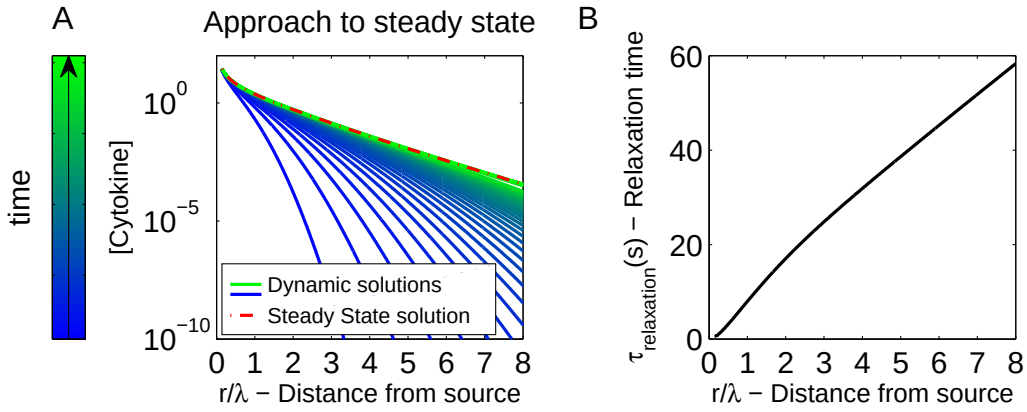

(A) Time dependent solutions of the 3D diffusion consumption equation (eq. 1) taking $\lambda_{\text{niche}} = 100\mu$m. The solution rapidly convergences to the steady state solution. (B) The relaxation timescale, measured as the time at which concentrations reach $1 - e^{-1} \approx 63\%$ of the final concentration follows a mostly linear curve Gregor et al. (2007); Kolomeisky (2011) with the exception of very short distances where a the relaxation time is dominated by diffusion.This timescale is in the order of minutes for physiological conditions.

In this study, we will develop techniques that will allow us to measure the extent of paracrine signaling in both 1- and 3- dimensional systems. The basic equation (3) is identical and so is the definition of λ_{niche}. However, and as is to be expected, the different dimensionalities lead to different concentration profiles.

2.1.1 Paracrine signaling - General formalism: 1D

In some of our experiments, cells were arranged in a dense cylindrical column and were supplied exogenous cytokine from above. Due to its symmetry this system can be treated as 1-dimensional. For a 1D system, Eq. 3 becomes:

$$\begin{aligned} 0 &= \frac{\partial c^2}{\partial \tilde{x}^2} - f(c), \\ 0 &= \frac{1}{2}\frac{\partial}{\partial \tilde{x}}\left(\frac{\partial c}{\partial \tilde{x}}\right)^2 - \frac{\partial}{\partial \tilde{x}}F(c), \qquad \text{where } F(c) = \int_0^c f(c')dc'. \end{aligned} \tag{4}$$

Integrating, we get $\frac{\partial c}{\partial \tilde{x}} = \pm\sqrt{2\left(F(c)+\eta\right)}$, where η is some constant of integration. As cytokine is supplied exogenously and the length of the wells (L) is finite, the boundary conditions are given by $c(x=0) = c_0$ and $\frac{\partial c}{\partial x}|_{x=L} = 0$. Moreover, we will only deal with conditions in which the system is not saturated with cytokine. In these conditions, the concentration of cytokine at the bottom of the plug is $c(x = L) = 0$. Also, due to mass conservation, c would be a monotonously decaying function. Since $F(0) = 0$, combining these boundary conditions gives us $\eta = 0$ and simplifies the equation:

$$\frac{\partial c}{\partial \tilde{x}} = -\sqrt{2F(c)}, \tag{5}$$

where again, $\tilde{x} \equiv \frac{x}{\lambda_{\text{niche}}}$. This can be directly integrated provided $f(c)$ is known.

2.1.1.1 Example: 1D Linear consumption

As a simple example, we can take a case where the consumption is related linearly to the concentration of the cytokine $f(c) = c$. In this case $F(c) = \int_0^c c'dc' = \frac{c^2}{2}$. Plugging this term into equation 5 yields $\frac{\partial c}{\partial \tilde{x}} = -c$ and the solution $c(\tilde{x}) = c_0 e^{-\tilde{x}}$ or in natural units, $c(x) = c_0 e^{-\frac{x}{\lambda_{\text{niche}}}}$.

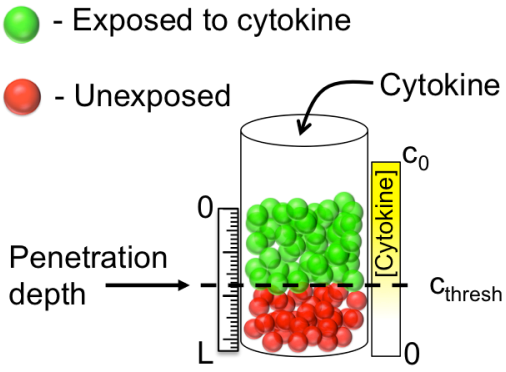

In 1 dimension, the fraction of cytokine exposed cells, and the penetration depth, are expected to scale as the concentration of consuming cells to the power $-\frac{1}{2}$.

We define a threshold concentration for detection c_{thresh} which will be determined by the specifics of the cellular response and the measuring device. The *penetration depth*, $x_{\text{penetration}}$, is the distance into the cell column in which the concentration is above c_{thresh}:

$$x_{\text{penetration}} = -\lambda_{\text{niche}} \int_{c_0}^{c_{\text{thresh}}} \frac{dc'}{\sqrt{2F(c')}} = \lambda_{\text{niche}} \int_{c_{\text{thresh}}}^{c_0} \frac{dc'}{\sqrt{2F(c')}} = \sqrt{\frac{\mathcal{D}}{k_{\text{consumption}} n_{\text{consumers}}}} \int_{c_{\text{thresh}}}^{c_0} \frac{dc'}{\sqrt{2F(c')}}. \tag{6}$$

Regardless of the specific form of $f(c)$, given the model assumptions of free diffusion and consumption by noninteracting cells, we expect the relation:

$$x_{\text{penetration}} \propto n_{\text{consumers}}^{-\frac{1}{2}}, \tag{7}$$

between the penetration depth and n, the concentration of consuming cells.

A similar scaling law naturally arises when we look at the fraction of the cells that were exposed to cytokine of the total cell population:

$$\text{Fraction exposed cells} = \frac{\text{\# Exposed cells}}{\text{\#Total cells}} = \frac{x_{\text{penetration}}}{L} \propto n_{\text{consumers}}^{-\frac{1}{2}}. \tag{8}$$

2.1.2 Paracrine signaling - General formalism: 3D

For a 3-dimensional system, assuming spherical symmetry, the diffusion-consumption equation is:

$$0 = \left(\frac{\partial^2}{\partial \tilde{r}^2} + \frac{2}{\tilde{r}}\frac{\partial}{\partial \tilde{r}}\right) c - f(c). \tag{9}$$

Under variable change $c(\tilde{r}) = \frac{q(\tilde{r})}{\tilde{r}}$ the equation becomes:

$$\frac{\partial^2 q}{\partial \tilde{r}^2} = \tilde{r} f\left(\frac{q}{\tilde{r}}\right) \tag{10}$$

Aside from the simplest cases, this nonlinear second order differential equation is not analytically tractable. Solutions for different forms of the function $f(\frac{q}{\tilde{r}})$ could be attained numerically (see section 3.2.1).

2.1.2.1 Example: 3D Linear consumption

One analytically solvable example is again the case of a linear consumption term $f(c) = c$ and a source of radius R generating a concentration c_0 on its surface. In this case $\frac{\partial^2 q}{\partial \tilde{r}^2} = q$. Taking the boundary conditions $q(\tilde{r} = \tilde{R}) \equiv q_0$ and $q(\tilde{r} \to \infty) = 0$ this leads to $q = q_0 \cdot e^{-(\tilde{r}-\tilde{R})}$, or $c(\tilde{r}) = \frac{c_0 \tilde{R}}{\tilde{r}} e^{-(\tilde{r}-\tilde{R})}$ or in natural units, $c(r) = \frac{c_0 R}{r} e^{-\frac{(r-R)}{\lambda_{\text{niche}}}}$.

This situation is mathematically identical to the case of Debye-Huckel screening in classical electrostatics Debye and Hückel (1923). The solution in that context is known as the screened Coulomb potential. In the context of atomic physics it is known as the Yukawa potential Yukawa (1955).

2.1.3 Estimation of λ_{niche} for the IL-2 system

Going back to the steady state diffusion consumption equation (Eq. 2) reintroducing the original units, along with the function $f(c) = c^* \frac{1}{1+\frac{c^*}{c}}$ we have.

$$0 = \nabla^2 c - \frac{k_{\text{consumption}} n_{\text{consumers}} c^*}{\mathcal{D}} \frac{1}{1+\frac{c^*}{c}}. \tag{11}$$

The maximal per-cell consumption rate is given by $A_{\text{max}} = k_{\text{consumption}} c^*$. We can estimate the value of λ_{niche} based on known parameters of the IL-2 system (table S1).

Parameter	Value	Source
$\mathcal{D}$	$100 \frac{\mu\text{m}^2}{s}$	Weidemann et al. (2011)
A_{max}	$0.3 - 1$ molecules per cell per second	Höfer et al. (2012); Yu et al. (2000); Weissman et al. (1986)
$n_{\text{consumers}}$	$\frac{1}{(10\mu\text{m})^3}$	Figure S1.D, for a system containing only consumers.
c^*	10pM	Höfer et al. (2012)

Table S1: Parameters for estimating λ_{niche} in the IL-2 system.

$$\lambda_{\text{niche}} = \sqrt{\frac{\mathcal{D}}{k \cdot n}} = \sqrt{\frac{\mathcal{D}c^*}{A_{\max} \cdot n}} = \\ \approx \sqrt{\frac{100[\frac{\mu\text{m}^2}{s}] \times 10[\text{pM}]}{1[\frac{1}{s}] \times \frac{1}{2}\frac{1}{1000}[\frac{1}{\mu\text{m}^3}]}} = \sqrt{\frac{100[\frac{\mu\text{m}^2}{s}] \times 10 \cdot 10^{-12} \cdot 2 \cdot 6 \cdot 10^{23} \cdot 10^{-15}[\frac{1}{\mu\text{m}^3}]}{1[\frac{1}{s}] \times \frac{1}{1000}[\frac{1}{\mu\text{m}^3}]}} \\ = \sqrt{1200[\mu\text{m}^2]} \approx 35\mu\text{m} = 3.5 \text{ cell diameters} \tag{12}$$

$$\lambda_{\text{niche}} = \sqrt{\frac{\mathcal{D}}{k_{\text{consumption}} \cdot n_{\text{consumers}}}} = \sqrt{\frac{\mathcal{D}c^*}{A_{\max} \cdot n_{\text{consumers}}}} \approx 25 - 45\mu\text{m} = 2.5 - 4.5 \text{ cell diameters} \tag{13}$$

So we expect to get a screening length λ_{niche} in the range of 2.5-4.5 cell diameters for a system with 100% IL-2 consumers in a dense configuration. This value should decrease as $\lambda_{\text{niche}} \sim n^{-\frac{1}{2}}$ as we change the density of consuming cells, n. This means that in physiological conditions, where the density of IL-2 consuming regulartory T cells is $\approx 10\%$ we expect $\lambda_{\text{niche}} \approx 8 - 14$ cell diameters.

3 Theory and Data analysis

3.1 1D Cytokine penetration, pSTAT5 response

Now, we can apply this general formalism described in section 2.1.1 to the case of cellular response to IL-2 measured by phosphorylation of STAT5. The specific shape of the $f(c)$ is given by a hill function with hill coefficient 1 and $c^* \equiv \text{EC}_{50} \approx 10pM$ (Fig. 3) $f(c) = c^* \frac{1}{1+\frac{c^*}{c}}$. By simple integration we get $F(c) = c^{*2}\left(\frac{c}{c^*} - \ln\left(1 + \frac{c}{c^*}\right)\right)$

$$x_{\text{penetration}} = \sqrt{\frac{\mathcal{D}}{k_{\text{consumption}} n_{\text{consumers}}}} \int_{c_{\text{thresh}}}^{c_0} \frac{dc'}{c^* \sqrt{2\left(\frac{c'}{c^*} - \ln\left(1 + \frac{c'}{c^*}\right)\right)}} \\ = \sqrt{\frac{\mathcal{D}}{k_{\text{consumption}} n_{\text{consumers}}}} \int_{\frac{c_{\text{thresh}}}{c^*}}^{\frac{c_0}{c^*}} \frac{dC'}{\sqrt{2(C' - \ln(1 + C'))}}. \tag{14}$$

We set the threshold concentration to correspond to 20% of the pSTAT5 MFI amplitude. This translates to $c_{\text{thresh}} = \frac{1}{4}c^*$. This threshold is chosen because it reflects the saddle-point of the distributions (Fig. 3). In fact, it could be chosen within a wide range of reasonable values without affecting the outcome.

$$x_{\text{penetration}} = \sqrt{\frac{\mathcal{D}}{k_{\text{consumption}} n_{\text{consumers}}}} \int_{\frac{1}{4}}^{\frac{c_0}{c^*}} \frac{dC'}{\sqrt{2(C' - \ln(1 + C'))}} \\ \equiv \sqrt{\frac{\mathcal{D}}{k_{\text{consumption}} n_{\text{consumers}}}} I\left(\frac{c_0}{c^*}\right) = \lambda_{\text{niche}} I\left(\frac{c_0}{c^*}\right). \tag{15}$$

The integral $I(\frac{c_0}{c^*}) \equiv \int_{\frac{1}{4}}^{\frac{c_0}{c^*}} \frac{dC'}{\sqrt{2(C' - \ln(1+C'))}}$ can be interpreted as the cytokine penetration depth in units of the screening length λ_{niche}. Although we will not use this approximation, we note that in the limit $c_0 \gg c^*$ this integral can be approximated as $I(\frac{c_0}{c^*}) \xrightarrow{c_0 \gg c^*} \sqrt{2\frac{c_0}{c^*}}$. As the source concentration increases, cells that are deeper into the plug are exposed to concentrations high enough for signaling:

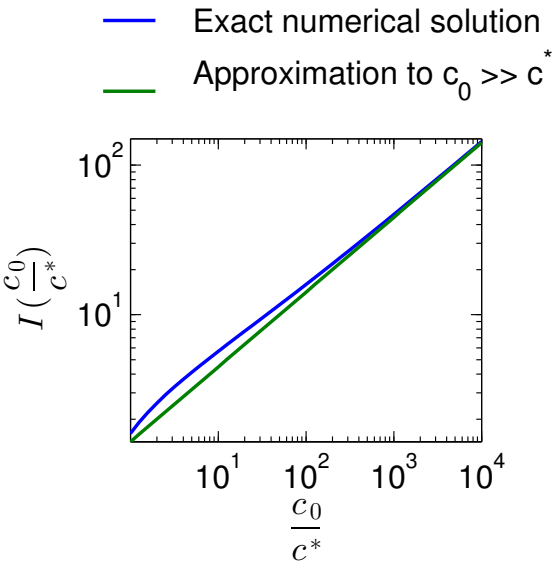

3.2 Imaging pSTAT5 response in vitro

Images were processed by segmenting individual cells by performing watershed segmentation Gonzalez and Woods (2007), then determining whether each cell is a consumer based on IL-2Rα expression. On each consumer, the total level of pSTAT5 expression and the center-of-mass is calculated and logged. Profiles of pSTAT5 expression on individual cells as a function of distance from the nearest producer are then generated.

3.2.1 Fitting procedure

pSTAT5 profiles (Fig. 4) are calculated using the numerical solution of equation 9. IL-2 consumption obeys a Hill function form with Hill coefficient 1 and $c^* \equiv \mathrm{EC}_{50} \approx 10pM$ (Fig. 3) $f(c) = c^* \frac{1}{1+\frac{c^*}{c}}$, giving the equation:

$$0 = \left(\frac{\partial^2}{\partial \tilde{r}^2} + \frac{2}{\tilde{r}} \frac{\partial}{\partial \tilde{r}} \right) \frac{c}{c^*} - \frac{1}{1+\frac{c^*}{c}}. \tag{16}$$

The response is calculated as pSTAT5$\propto \frac{1}{1+\frac{c^*}{c}}$ with the proportionality constant determined experimentally.

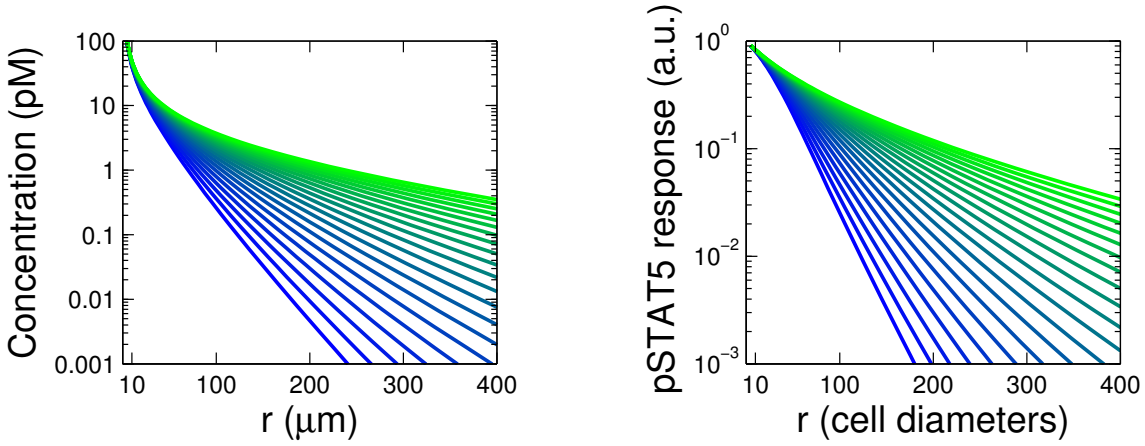

Numerical solutions of the spherically symmetric diffusion-consumption equations in 3 dimensions for λ_{niche} in the range 3 (bluest) to 30 (greenest) cell diameters . Left: cytokine concentration profile. Right: cellular response.

These solutions are then used as fitting functions for the measured pSTAT5 response. The fitting parameters are the screening length λ_{niche}, and the production rate of the sources.

3.3 Imaging pSTAT5 response in vivo

Analysis of in vivo images is done by segmenting individual T_{regs} and AdTr producers. For each T_{reg} we log the position and pSTAT5 fluorescence. Since cytokine signals can permeate from sources outside of the current slice, it is best to analyze these images by quantifying the size of pSTAT5$^+$ clusters in the tissue. This is achieved by calculating the pSTAT5 autocorrelation function $c(r) = \langle \text{pSTAT5}(R)\text{pSTAT5}(R+r)\rangle$ where averages are taken over all positions R. Due to the complex structures and variable sizes of spleen nodules, calculating the autocorrelation function yields unreliable results. We therefore focused this analysis on the lymph nodes, which have larger and more homogeneous T-cell zones.

3.3.1 pSTAT5 autocorrelation function

We denote the pSTAT5 concentration field surrounding one producing cell by $\phi(\mathbf{r})$. Since in practice the concentration fields appear to be close to or below EC_{50} (Fig. 4) we will make the following two assumptions:

1. The field generated by a single producer $\phi(\mathbf{r})$ can be approximated to a Yukawa term (section 2.1.2.1).
2. For low densities of producers, fields can be combined by superposition.

The concentration of cytokine at some point $\mathbf{r}$ will be a superposition of cytokines emanating from all the producing cells in the environment: $c(\mathbf{r}) = \int n_{\text{p}}(\mathbf{r}')\phi(\mathbf{r}-\mathbf{r}')d\mathbf{r}'$, where we denote the density of producing cells by n_p. The autocorrelation function is defined as

$$G(r) = \langle c(0)c(\mathbf{r})\rangle = \int \phi(-\mathbf{r}')\phi(\mathbf{r}-\mathbf{r}'')\langle n_{\text{p}}(\mathbf{r}')n_{\text{p}}(\mathbf{r}'')\rangle d\mathbf{r}'d\mathbf{r}''. \tag{17}$$

At low densities of producers, there is no correlation in the positions of different sources :$\langle n_{\text{p}}(\mathbf{r}')n_{\text{p}}(\mathbf{r}'')\rangle = \bar{n}_{\text{p}}\delta(\mathbf{r}'-\mathbf{r}'')$ (data not shown). We show this experimentally by calculating the source-source correlation function in lymph nodes sections collected from mice that were adoptively transferred with 5×10^5 5C.C7 T cells, in IL-2i.c. boosted and wild type conditions.

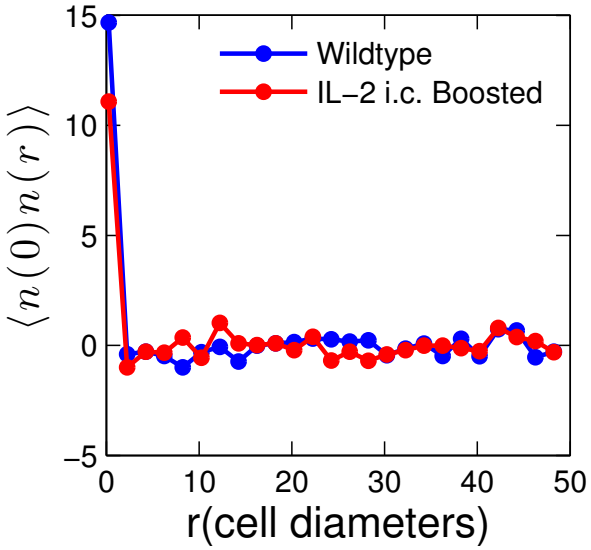

By remembering that $\phi(\mathbf{r}) = \phi(|\mathbf{r}|)$ we get

$$\begin{aligned}\langle c(0)c(\mathbf{r})\rangle &= \int \phi(\mathbf{r}')\phi(\mathbf{r}-\mathbf{r}'')\bar{n}_{\text{p}}\delta(\mathbf{r}'-\mathbf{r}'')d\mathbf{r}'d\mathbf{r}'',\\ &= \bar{n}_{\text{p}}\int \phi(\mathbf{r}')\phi(\mathbf{r}-\mathbf{r}')d\mathbf{r}' = \bar{n}_{\text{p}}(\phi*\phi)(\mathbf{r}),\end{aligned} \tag{18}$$

where $(\cdot * \cdot)$ denotes a convolution. To perform this convolution we will calculate the Fourier transform of the function $\phi(\mathbf{r})$: $\tilde{\phi}(\mathbf{q}) = \frac{1}{(2\pi)^{\frac{3}{2}}} \int \phi(\mathbf{r}) e^{-i\mathbf{q}\cdot\mathbf{r}} d\mathbf{r}$, square it in Fourier space, and then perform the inverse transform:

$$\langle c(0)c(\mathbf{r})\rangle = \bar{n}_{\mathrm{p}} \int \left|\tilde{\phi}(\mathbf{q})\right|^2 e^{i\mathbf{q}\cdot\mathbf{r}} d\mathbf{q}. \tag{19}$$

For the case of linear receptors ($[IL-2] < \mathrm{EC}_{50}$) the single-source-field is given by a Yukawa term $\phi(\mathbf{r}) = \frac{Q}{r} e^{-\frac{r}{\lambda_{\mathrm{niche}}}}$. We perform a Fourier transform to get

$$\tilde{\phi}(\mathbf{q}) = \frac{1}{(2\pi)^{\frac{3}{2}}} \int \phi(\mathbf{r}) e^{-i\mathbf{q}\cdot\mathbf{r}} d\mathbf{r} = \frac{1}{(2\pi)^{\frac{3}{2}}} \int_0^\infty Q e^{-\frac{r}{\lambda_{\mathrm{niche}}}} r dr \int e^{-i\mathbf{q}\cdot\mathbf{r}} d\Omega. \tag{20}$$

The angular integral can be solved directly $\int e^{-i\mathbf{q}\cdot\mathbf{r}} d\Omega = 2\pi \int_0^\pi e^{-iqr\cos\theta} \sin\theta d\theta = 4\pi \frac{\sin(qr)}{qr}$ and plugged back into equation 20 to yield

$$\tilde{\phi}(\mathbf{q}) = \sqrt{\frac{2}{\pi}} \frac{Q}{q} \int_0^\infty e^{-\frac{r}{\lambda_{\mathrm{niche}}}} \sin(qr) dr = \sqrt{\frac{2}{\pi}} \frac{Q}{q^2} \int_0^\infty e^{-\frac{r}{q\lambda_{\mathrm{niche}}}} \sin(r) dr = \sqrt{\frac{2}{\pi}} \frac{Q}{q^2} \frac{1}{1+\frac{1}{q^2\lambda_{\mathrm{niche}}^2}}. \tag{21}$$

Now, we can return the term for $\phi(\mathbf{q})$ into equation 19 which gives:

$$\begin{aligned}\langle c(0)c(\mathbf{r})\rangle &= \bar{n}_{\mathrm{p}} \frac{2Q^2\lambda_{\mathrm{niche}}^4}{\pi} \int \left|\frac{1}{1+q^2\lambda_{\mathrm{niche}}^2}\right|^2 e^{i\mathbf{q}\cdot\mathbf{r}} d\mathbf{q} \\ &= \bar{n}_{\mathrm{p}} \frac{2Q^2\lambda_{\mathrm{niche}}^4}{\pi} \int_0^\infty \frac{1}{(1+q^2\lambda_{\mathrm{niche}}^2)^2} q^2 dq \int e^{i\mathbf{q}\cdot\mathbf{r}} d\Omega \end{aligned} \tag{22}$$

Using the same angler integral as before we get:

$$\langle c(0)c(\mathbf{r})\rangle = \bar{n}_{\mathrm{p}} \frac{8Q^2\lambda_{\mathrm{niche}}^4}{r} \int_0^\infty \frac{\sin(qr)}{(1+q^2\lambda_{\mathrm{niche}}^2)^2} q dq. \tag{23}$$

Now, to solve this integral we first perform integration by parts:

$$\begin{aligned}\int_0^\infty \frac{\sin(qr)}{(1+q^2\lambda_{\mathrm{niche}}^2)^2} q dq &= -\frac{1}{2\lambda_{\mathrm{niche}}^2} \int_0^\infty \sin(qr) d\left(\frac{1}{1+q^2\lambda_{\mathrm{niche}}^2}\right) \\ &= -\cancel{\frac{1}{2\lambda_{\mathrm{niche}}^2} \sin(qr) \left(\frac{1}{1+q^2\lambda_{\mathrm{niche}}^2}\right)\Big|_0^\infty} + \frac{r}{2\lambda_{\mathrm{niche}}^2} \int_0^\infty \frac{\cos(qr)}{1+q^2\lambda_{\mathrm{niche}}^2} dq. \end{aligned} \tag{24}$$

The only remaining integral is $I(r) = \int_0^\infty \frac{\cos(qr)}{1+q^2\lambda_{\mathrm{niche}}^2} dq$. This Fourier transform of a Lorentzian can be estimated using Cauchy's formula:

$$I(r) = \int_0^\infty \frac{\cos(qr)}{1+q^2\lambda_{\mathrm{niche}}^2} dq = \frac{1}{2}\mathcal{R}e\left(\int_{-\infty}^\infty \frac{e^{iqr}}{1+q^2\lambda_{\mathrm{niche}}^2} dq\right) = \frac{1}{2\lambda_{\mathrm{niche}}^2}\mathcal{R}e\left(\int_{-\infty}^\infty \frac{\frac{e^{iqr}}{q+\frac{i}{\lambda_{\mathrm{niche}}}}}{q-\frac{i}{\lambda_{\mathrm{niche}}}} dq\right) \tag{25}$$

$$= \frac{1}{2\lambda_{\mathrm{niche}}^2}\mathcal{R}e\left(\oint \frac{\frac{e^{izr}}{z+\frac{i}{\lambda_{\mathrm{niche}}}}}{z-\frac{i}{\lambda_{\mathrm{niche}}}} dz\right) = -\frac{1}{2\lambda_{\mathrm{niche}}^2} \times 2\pi i \times \frac{e^{-\frac{r}{\lambda_{\mathrm{niche}}}}}{-\frac{2i}{\lambda_{\mathrm{niche}}}} = \frac{\pi}{2\lambda_{\mathrm{niche}}} e^{-\frac{r}{\lambda_{\mathrm{niche}}}}. \tag{26}$$

Finally, we plug together equations 23, 24, and 25 to get the correlation function

$$G(r) = \langle c(0)c(\mathbf{r})\rangle = 2\pi Q^2 \bar{n}_{\mathrm{p}} \lambda_{\mathrm{niche}} e^{-\frac{r}{\lambda_{\mathrm{niche}}}} \propto e^{-\frac{r}{\lambda_{\mathrm{niche}}}}. \tag{27}$$

We see that the correlation function is expected to follow a simple exponential decay, with the decay coefficient being λ_{niche}, the screening length.

4 Extended Methods

4.1 Antibodies and Reagents

α-CD4 clone RM4-5, Alexa700, Pacific Blue, BD Bioscience
α-IL-2Rα clone PC61, PECy7, PerCPCy5.5, BD Bioscience
α-IL-2Rα clone 7D4, PE, Miltenyi Biotec
α-Foxp3 clone MF23, PE, Biolegend
α-IL-2 clone JES6-1A12, eBioscience
α-IL-2 clone JES6-5H4, PE, APC, purified, eBioscience
Primary antibody rabbit α-phospho-STAT5 (pY694) clones C11C5 (for FC), C71E5 (for IF), Cell Signaling
Primary antibody rabbit α-phospho-STAT1 (pY701) clone 58D6, Cell Signaling
Primary antibody rabbit α-phospho-STAT6 (pY641), Cell Signaling
Secondary polyclonal antibody α-rabbit IgG, Alexa 488, FITC, PE, APC, Jackson ImmunoResearch
Secondary polyclonal antibody α-rat TRITC Jackson ImmunoResearch
Mouse CD4 (L3T4) MicroBeads, Miltenyi Biotec
Mouse IL-2 Secretion Assay Kit, Miltenyi Biotec
FoxP3 fixation/permeabilization kit, eBioscience
Recombinant mouse IL-2, eBioscience
Recombinant human IL-2, Amgen
Recombinant mouse IFNγ, GenScript
Recombinant mouse IL-4, eBioscience
K5 peptide (ANERADLIAYFKAATKF), GenScript
Lipopolysaccharide from *Salmonella typhimurium*, Sigma
Cell Trace Violet (CTV) and Cell Trace Far-Red (DDAO), Molecular Probes
AZD1480, the chemical inhibitor of JAK1/JAK2 was a gift from Dr Jackie Bromberg (MSKCC)
Phorbol 12-myristate 13-acetate (PMA) and Ionomycin, Sigma
Silicone rubber compound RTV615 (PDMS), Momentive
Ficoll-paque plus, GE Healthcare
Triton-100X, MP Biomedicals
Poly-l-lysine solution, Sigma
Fluoromount Aqueous Mounting Medium, Sigma
Phosphate Buffered Saline, Sigma

4.2 Clusterwell plates

Due to the typically low densities of cells in suspension, along with the media and the cells ability to rapidly mix, localization due to density-dependent consumption is not significant in typical cell culture conditions. Using centrifugation cells could be pelleted at a density comparable to that of solid tissue where the effect is expected to be strong. However, because of their geometry and size, standard multiwell plates are not suitable for a quantitative measurement of cytokine penetration. To this end, we fabricated a custom-designed device (Fig. 3, S2) which confines cells to a dense cluster, with simple cylindrical geometry, which we named the clusterwell plate. Cells can be added sequentially, creating a layered stack with different cellular compositions. The plates were designed to be compatible with standard lab equipment such as multi-channel pipetors and centrifuge plate holders (available upon demand).

4.2.1 Fabrication of Clusterwell plates

Fig. S1.A,B

An aluminum mold was fabricated at the Ben-Gurion University Physics Department machine shop. The mold was designed to create cylindrical wells with a 6mm diameter at their top. At the bottom of each well the diameter gradually shortens down to a smaller cylinder of 1mm diameter, resembling a small capped funnel.

The bottom of a 75 cm^2 polystyrene tissue culture flask (Greiner - 658170) was sawed off so as to create a small basin roughly 60mL in volume. Polydimethylsiloxane parts A and B were thoroughly mixed at a 10:1 ratio and degased.

40mL of liquid PDMS were added to the basin. After placing the aluminum mold the basin was put in a 75°C oven to cure overnight. The following morning the mold was removed, the cured PDMS was washed repeatedly with distilled water.

To create a cluster of packed cells, suspended cell cultures are transferred into clusterwells and then centrifuged for one minute at 400g. The cells will form a densely packed pellet at the bottom of the clusterwell.

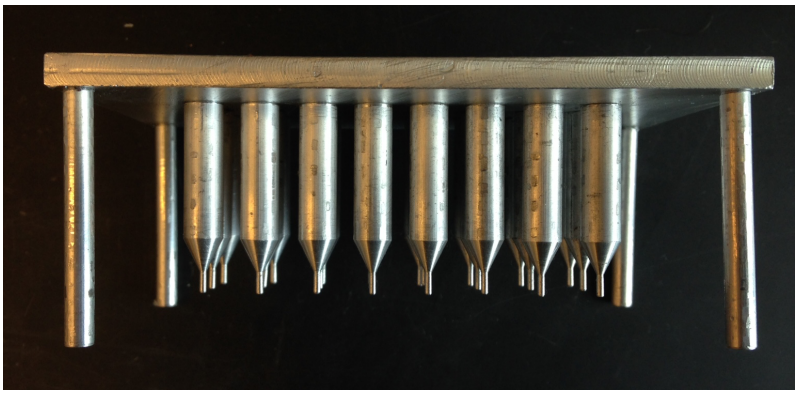

Aluminum mold used in the fabrication of the clusterwell plate.

4.3 Measuring and perturbing the cytokine penetration *in vitro* using the clusterwell plate

4.3.1 Quantifying cytokine penetration in 1D for varying densities of consuming cells.

Fig. 3, Fig. S1.C-F

For IL-2, B10.A splenocytes that were activated using 5ng/mL PMA and 500ng/mL Ionomycin and cultured in the presence of IL-2 for at least 4 days(IL-2Rα^+*consumers*) , were mixed at different ratios with "*inert*" cells harvested from T cell-deficient B10.A *Cd3e*$^{-/-}$ mice. To remove receptor-bound cytokines, consumer cells were exposed to 0.1M glycine at pH 4.0 for 1 minute on ice, followed by several washes with RPMI. Consumers were then rested for an hour at 37°C before being mixed with inert cells and loaded into the cluster well plate.

Without disturbing the pellets, exogenous IL-2 was added to the top of the cluster at a final concentration of 200pM. The cell clusters were incubated for 1 hour at 37°C, allowing signaling to reach steady state. Clusters were then rapidly fixed with cold 1.6% paraformaldehyde (PFA), permeabilized with 90% methanol (MeOH), and stored at -20°C. Cells were then stained with the appropriate antibodies and analyzed by flow cytometry.

4.3.2 Quantifying cytokine penetration in 1D from a varying cytokine source

Fig. S2

To measure the penetration of IL-2, B10.A splenocytes were activated and cultured in the presence of IL-2 (IL-2Rα^+*consumers*). To remove receptor-bound cytokines, consumer cells were exposed to 0.1M glycine at pH 4.0 for 1 minute on ice, followed by several washes with RPMI. Consumers were then rested for an hour at 37°C before being loaded into the cluster well plate.

To measure the penetration of IFNγ, B16-F10 melanoma cells, which express the IFNγ receptor but do not produce IFNγ were loaded into cluster wells.

To measure the penetration of IL-4, CH12 lymphoma cells, which express the IL-4 receptor but do not produce IL-4 were loaded into cluster wells.

Without disturbing the pellets, exogenous IL-2 ,IFNγ, or IL-4 was added to the top of clusters containing the relevant cell type to final concentrations of 10 nM, 1 nM, and 100 pM. The cell clusters were incubated for 1 hour at 37°C, allowing signaling to reach steady state. Clusters were then rapidly fixed with cold 1.6% paraformaldehyde (PFA), permeabilized with 90% methanol (MeOH), and stored at -20°C. Cells were then stained with the appropriate antibodies and analyzed by flow cytometry.

4.4 Measuring the dynamics of IL-2 secretion by single cells.

Fig. S3

$CD4^+$ T cells were isolated from C57BL/6 splenocytes using Mouse CD4 MicroBeads (Miltenyi Biotec). The cells were activated using 5ng/mL PMA and 500ng/mL Ionomycin and cultured in the presence of IL-2 for 5 days. On day 5, stained with Celltrace Violet (CTV, Molecular Probes) and coated with an IL-2 specific capture matrix (Miltenyi Biotec). A grid of microscopic (50x50x50 μm^3) wells made of polydimethylsiloxane Le Floc'h et al. (2013) were submerged in imaging media (standard media as described in the methods section, without phenol red). Cells were then seeded in the wells in the presence of 5ng/mL PMA and 500ng/mL Ionomycin ((Sigma-Aldrich) for restimulation), recombinant mouse IL-2 ((eBioscience) as a positive control), or DMSO ((Sigma-Aldrich) as a negative control) and anti-IL2-Alexa 488 (clone JES6-5H4), for detection of the cytokine. In general, individual wells contained 1-3 T cells. Cells were imaged using a 20x objective lens (Carl Zeiss) at 5-min intervals for 4 hours. Brightfield, CTV, and Alexa 488 images were collected at each time point. Quantification was restricted to wells containing one cytokine producer. This was adapted the experimental procedure from Huang et al. (2013).

4.5 Imaging cytokine concentration fields using PlaneView imaging devices

4.5.1 Preparation of cells for imaging

C57BL/6 T cells that were activated using 5ng/mL PMA and 500ng/mL Ionomycin and cultured in the presence of IL-2 for at least 4 days (IL-2Rα^+*consumers*) were mixed at different ratios with CD4 depleted naive C57BL/6 splenocytes (*inert cells*). To remove receptor-bound cytokines, consumer cells were exposed to 0.1M glycine at pH 4.0 for 1 minute on ice, followed by several washes with RPMI. Consumers were then rested for an hour at 37°C before being mixed with inert cells and loaded into the imaging device.

IL-2 producing cells ("Producers") were made by re-administering of 5ng/mL PMA and 500ng/mL Ionomycin activation protocol to previously activated T-cells cultures. This reactivation leads to a rapid and extensive production of IL-2 by the T-cells. These cells were labeled with DDAO-SE at 1μM for subsequent identification.

4.5.2 Fabrication of PlaneView imaging devices

Glass slides (Menzel-Gälser) were coated with poly-l-lysine for 40 minutes at 37°C, washed with H_2O and allowed to dry at room temperature for 1 hour. A small (ϕ6mm) hollow cylinder made of PDMS was placed on the slide, the PDMS rapidly attaches to the slide creating a small well.

To create a tightly packed cell pellet, cell suspensions are added into the PDMS well and the device is centrifuged for 1 minute at 800$\times$g to allow cells to stick to the glass slide. The PDMS well is then removed and a semipermeable membrane with 400nm pores is carefully placed on top of the cells. This membrane protects the cells from moving due to changing reagents, and prevents convection flows from distorting the concentration fields. The cells and membrane are then covered by a larger PDMS well (ϕ12mm) to allow for the confinement of reagents around the cells.

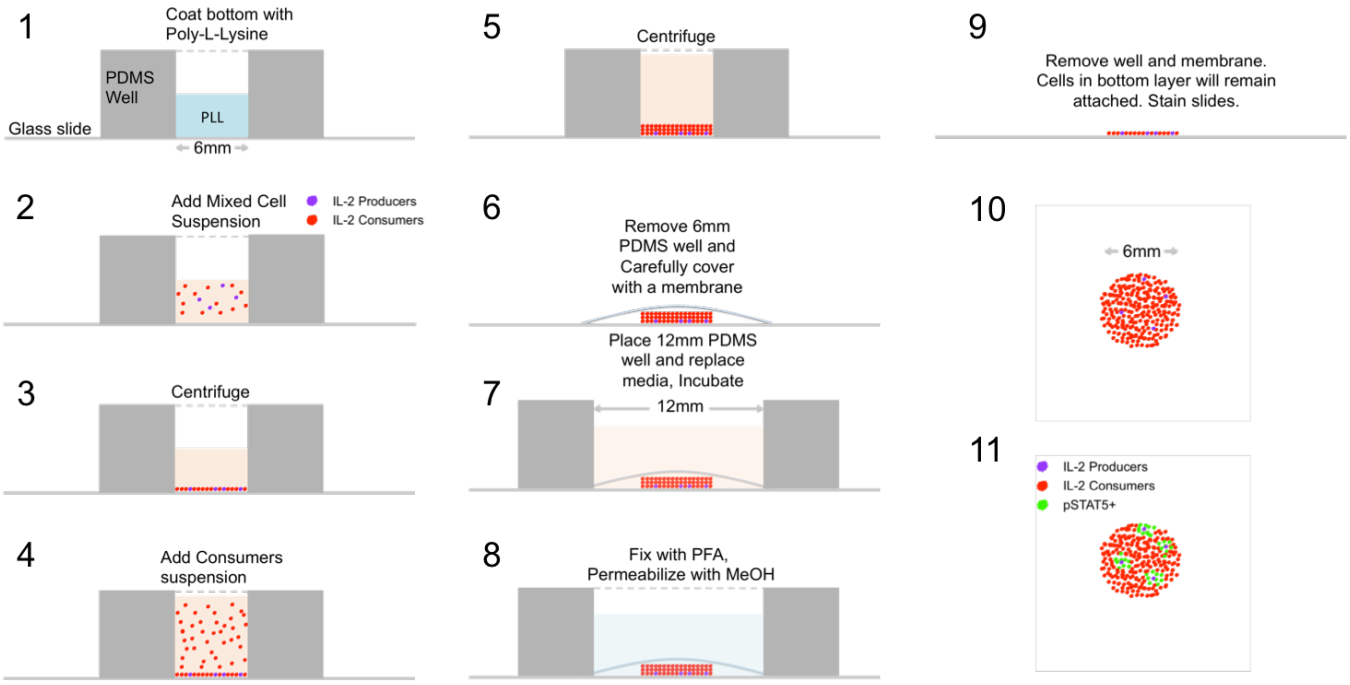

Preparation of the PlaneView imaging devices is done by first coating a glass slide with Poly-L-Lysine (1). Then, a cell suspension containing a small fraction of cytokine producing cells is deposited in a monolayer by centrifugation(2,3). 10 layers of cells containing no producers is deposited on top to form a 3 dimensional structure(4,5). The cells are covered with a semipermeable membrane (6), incubated for 1 hour (7), and fixed in situ(8). Cells are then permeabilized and stained for pSTAT5 signaling(9,10).

4.5.3 In vitro imaging of cytokine concentration fields using PlaneView imaging devices

Fig. 4, Fig. S2, Fig. S4

IL-2 consuming T cells, or a combination of 10% consuming T cells and 90% inert cells were mixed with 0.1% IL-2 producing T cells and deposited in a monolayer. Then, 10 more layers of cells containing no producers were added on top, forming a three dimensional array with the producing cells dispersed on the bottom, a semipermeable membrane was placed on the cells to preserve their positions during further processing.

To control for background STAT5 (Fig S4.C) phosphorylation and for IL-2 specificity, devices were loaded with consuming cell cultures containing no producers. The cells were then covered with either fresh media or with media containing 10nM IL-2 to serve as negative and positive controls, respectively.

The system is allowed 1 hour to reach a steady state. After that, the cells are fixed for 15 minutes with warm 4% PFA and made permeable using ice cold 90% MeOH for 10 minutes to allow for intracellular immunostaining. After fixation and permeabilization the PDMS well and the membrane are removed, at this stage the cells would be tightly bound to the glass slide and standard immunostaining protocols can be used. Non specific antibody binding is blocked by a 1 hour incubation in 5% FBS and 0.3% Triton X-100 in PBS at room temperature. Primary antibodies (Rabbit anti-pSTAT5 1:200) are applied in a moist chamber for 1 hour at room temperature. Fluorophore conjugated antibodies (Goat anti-Rabbit Alexa 488, Rat anti-IL-2Rα R-PE, 1:300) are applied for 1 hour at room temperature. Cells are then briefly stained with DAPI and a coverslip is mounted using Fluoromount Aqueous Mounting Medium (Sigma) for epi-fluorescent imaging.

References

Boyman, O. and Sprent, J. (2012), 'The role of interleukin-2 during homeostasis and activation of the immune system.', *Nature reviews. Immunology* **12**(3), 180–90.

Debye, P. and Hückel, E. (1923), 'Zur Theorie der Elektrolyte. I. Gefrierpunktserniedrigung und verwandte Erscheinungen. The theory of electrolytes. I. Lowering of freezing point and related phenomena', *Physikalische Zeitschrift* **24**, 185 – 206.

Gonzalez, R. C. and Woods, R. E. (2007), *Digital Image Processing (3rd Edition)*.

Gregor, T., Wieschaus, E. F., McGregor, A. P., Bialek, W. and Tank, D. W. (2007), 'Stability and nuclear dynamics of the bicoid morphogen gradient.', *Cell* **130**(1), 141–52.

Helmstetter, C., Flossdorf, M., Peine, M., Kupz, A., Zhu, J., Hegazy, A. N., Duque-Correa, M. A., Zhang, Q., Vainshtein, Y., Radbruch, A., Kaufmann, S. H., Paul, W. E., Höfer, T. and Löhning, M. (2015), 'Individual T helper cells have a quantitative cytokine memory.', *Immunity* **42**(1), 108–22.

Höfer, T., Krichevsky, O. and Altan-Bonnet, G. (2012), 'Competition for IL-2 between Regulatory and Effector T Cells to Chisel Immune Responses.', *Frontiers in immunology* **3**, 268.

Huang, J., Brameshuber, M., Zeng, X., Xie, J., jing Li, Q., hsiu Chien, Y., Valitutti, S. and Davis, M. M. (2013), 'A Single peptide-major histocompatibility complex ligand triggers digital cytokine secretion in CD4+ T Cells', *Immunity* **39**(5), 846–857.

Jacob, J. (1991), 'In situ studies of the primary immune response to (4-hydroxy-3- nitrophenyl)acetyl. I. The architecture and dynamics of responding cell populations', *Journal of Experimental Medicine* **173**(5), 1165–1175.

Janský, L., Reymanová, P. and Kopecký, J. (2003), 'Dynamics of cytokine production in human peripheral blood mononuclear cells stimulated by LPS or infected by Borrelia.', *Physiological research / Academia Scientiarum Bohemoslovaca* **52**(5), 593–8.

Kolomeisky, A. B. (2011), 'Formation of a Morphogen Gradient: Acceleration by Degradation', *The Journal of Physical Chemistry Letters* **2**(13), 1502–1505.

Le Floc'h, A., Tanaka, Y., Bantilan, N. S., Voisinne, G., Altan-Bonnet, G., Fukui, Y. and Huse, M. (2013), 'Annular PIP3 accumulation controls actin architecture and modulates cytotoxicity at the immunological synapse', *Journal of Experimental Medicine* **210**(12).

Murphy, K. (2011), *Janeway's Immunobiology (Immunobiology: The Immune System (Janeway))*, Garland Science.

Sojka, D. K., Bruniquel, D., Schwartz, R. H. and Singh, N. J. (2004), 'IL-2 Secretion by CD4+ T Cells In Vivo Is Rapid, Transient, and Influenced by TCR-Specific Competition', *The Journal of Immunology* **172**(10), 6136–6143.

Tkach, K. E., Barik, D., Voisinne, G., Malandro, N., Hathorn, M. M., Cotari, J. W., Vogel, R., Merghoub, T., Wolchok, J., Krichevsky, O. and Altan-Bonnet, G. (2014), 'T cells translate individual, quantal activation into collective, analog cytokine responses via time-integrated feedbacks.', *eLife* **3**, e01944.

Weidemann, T., Worch, R., Kurgonaite, K., Hintersteiner, M., Bökel, C. and Schwille, P. (2011), 'Single Cell Analysis of Ligand Binding and Complex Formation of Interleukin-4 Receptor Subunits', *Biophysical Journal* **101**(10), 2360–2369.

Weissman, A. M., Harford, J. B., Svetlik, P. B., Leonard, W. L., Depper, J. M., Waldmann, T. A., Greene, W. C. and Klausner, R. D. (1986), 'Only high-affinity receptors for interleukin 2 mediate internalization of ligand.', *Proceedings of the National Academy of Sciences of the United States of America* **83**(5), 1463–6.

Yu, A., Olosz, F., Choi, C. Y. and Malek, T. R. (2000), 'Efficient Internalization of IL-2 Depends on the Distal Portion of the Cytoplasmic Tail of the IL-2R Common -Chain and a Lymphoid Cell Environment', *The Journal of Immunology* **165**(5), 2556–2562.

Yukawa, H. (1955), 'On the Interaction of Elementary Particles. I *', *Progress of Theoretical Physics Supplement* **1**, 1–10.